A Search for Early Optical Emission from Short and Long Duration Gamma-ray Bursts

Robert Kehoe[1,4], Carl Akerlof[1], Richard Balsano[2], Scott Barthelmy[5], Jeff Bloch[2], Paul Butterworth[5], Don Casperson[2], Tom Cline[5], Sandra Fletcher[2], Galen Gisler[2], Kevin Hurley[7], Marc Kippen[6], Brian Lee[1,8], Stuart Marshall[3], Tim McKay[1], Eli Rykoff[1], Don Smith[1], Tom Vestrand[2] and Jim Wren[2]

[1]*University of Michigan, Ann Arbor, MI 48109*

[2]*Los Alamos National Laboratory, Los Alamos, NM 87545*

[3]*Lawrence Livermore National Laboratory, Livermore, CA 94550*

[4]*Michigan State University, East Lansing, MI 48824*

[5]*NASA/Goddard Space Flight Center, Greenbelt, MD 20771*

[6]*NASA/Marshall Space Flight Center, Huntsville, AL 35805*

[7]*Space Sciences Laboratory, University of California, Berkeley, CA 94720-7450*

[8]*Fermi National Accelerator Laboratory, Batavia, IL 60510*

ABSTRACT

Gamma-ray bursts of short duration may harbor vital clues to the range of phenomena producing bursts. However, recent progress from the observation of optical counterparts has not benefitted the study of short bursts. We have searched for early optical emission from six gamma-ray bursts using the ROTSE-I telephoto array. Three of these events were of short duration, including GRB 980527 which is among the brightest short bursts yet observed. The data consist of unfiltered CCD optical images taken in response to BATSE triggers delivered via the GCN. For the first time, we have analyzed the entire $16^\circ \times 16^\circ$ field covered for five of these bursts. In addition, we discuss a search for the optical counterpart to GRB 000201, a well-localized long burst. Single image sensitivities range from 13th to 14th magnitude around 10 s after the initial burst detection, and 14 - 15.8 one hour later. No new optical counterparts were discovered in this analysis suggesting short burst optical and gamma-ray fluxes are uncorrelated.

Subject headings: gamma rays: bursts, observations

1. Introduction

During the last decade, gamma-ray burst classification has emerged as a promising tool to understand these events. In the pre-BATSE data, there were indications of a bimodality in the temporal durations of non-repeating bursts (Hurley 1992), as well as a modest correlation of duration with spectral hardness (Dezalay et al. 1992). These results were confirmed by data from the Burst and Transient Source Experiment (BATSE) which show that short bursts inhabit a distinct region of the duration/spectral hardness parameter space (Kouvelioutou et al. 1993). More recently, theoretical work has made use of the BATSE archive to attempt to determine the processes which distinguish short and long bursts. There is some evidence that short GRBs arise from internal shock processes (Nakar and Piran 2001), and that they are differentiated from long bursts by the ejecta shell geometry (eg. (Kobayashi 2000)). Alternatively, these two classes may arise from different accretion disk states around progenitor black holes (van Putten and Ostriker 2001). Indications that very short bursts exhibit an unusually uniform spectral hardness distribution may hint at yet a third class of GRB (Cline et al. 1999).

Despite what has been gleaned from the gamma-ray emission, the study of short bursts has not been benefited by the more recent advances brought about by optical afterglow (eg. (Metzger et al. 1997), (Kulkarni et al. 1998)) and burst (Akerlof et al. 1999) observations, all of which have identified only long-duration bursts. One of the main reasons for this bias stem from difficulty in obtaining well-localized final positions for these events. To date, the main source of well-localized burst notices for late optical study has been the BeppoSAX satellite (Feroci et al. 1997), but the 1 s integration time of the GRBM prevents efficient detection of short bursts. In addition, prompt wide-field searches such as ROTSE-I and LOTIS (Park et al. 1999) have been hampered by the practical difficulty of searching their ˜250 sq. degree fields. At a sensitivity of 15th magnitude, there are of order 10^5 stars in these fields, and approximately a few million photometric measurements in a typical ROTSE-I trigger response. Burst finding necessitates well-controlled photometry across an entire field, as well as a detailed knowledge of the hardware behavior (eg. bad pixels, position resolution). Although this limitation was overcome for long bursts by using localizations from the Inter-Planetary Network (IPN, (Hurley et al. 1999)) to reduce the search area (Akerlof et al. 2000), no such localizations were available for the short bursts on which ROTSE-I triggered.

To overcome this limitation, we have designed an analysis specifically to confidently analyze many observations of a large field. This paper presents the results of a search for optical counterparts to five bursts in the ROTSE-I trigger data sample using these techniques. An additional burst, studied with our previous method, is also presented.

2. Observations and Reduction

The ROTSE-I array used in these observations consists of four telephoto lenses comounted in a 2×2 geometry on a lightweight platform which allows rapid slews and excellent pointing accuracy relative to the $16.4^o \times 16.4^o$ total field-of-view (14.4" pixel scale, see (Kehoe et al. 2000a) for more details). From March, 1998 until the deorbiting of the Compton Gamma-Ray Observatory (CGRO) in June 2000, 57 GRB triggers were received via the GRB Coordinates Network (GCN, (Barthelmy et al. 1998), (Barthelmy et al. 1995)) derived from BATSE data (Paciesas et al. 1999). To date, we have successfully analyzed data for a subset of seven long duration bursts possessing small localization errors, yielding one detected prompt optical counterpart (Akerlof et al. 1999) and six non-detections (Akerlof et al. 2000). This paper discusses a search in a set of six additional triggers taken during the full period of BATSE activity while ROTSE-I was automated. Five of these triggers were selected for this analysis because (1) they fall into the short duration class of bursts, (2) their most probable known position is within 5^o of the ROTSE-I pointing, or (3) we have a thorough, photometric-quality set of images from most of the cameras. The sixth burst, GRB 000201, is included because the analysis of the known IPN diamond localizing this burst was straightforward, and other optical follow-up has been performed (Boer et al. 2000). Preliminary results for GRB 980527 and GRB 000201 have been previously presented in (Kehoe et al. 2000a; Kehoe et al. 2000b), respectively. This paper supersedes and improves upon those results. Some important burst parameters from the BATSE observations, as well as the ROTSE-I spatial and temporal coverages are itemized in Table 1. The spatial coverage is defined as the probability that the burst location was imaged in our search, and it is based on the statistical and systematic uncertainties in the best BATSE or IPN localizations.

The observations scheduled in response to a trigger vary somewhat depending on trigger type and delay from the time of the burst. The three trigger types involved in this analysis are 'Original' which arrives around 7 seconds after the burst start, 'Final' which arrives approximately 1 minute later, and 'MAXBC' which arrives about 5 to 10 minutes after the burst. For all of the trigger responses taken with ROTSE-I, 5 s exposures are taken during the first minute of the burst. Prior to December 1998, the exposures were lengthened to 25 s and then 125 s as the delay progressed from 1 minute to approximately 10 minutes. After January 1999, these longer exposure lengths were reduced to 20 s and 80 s, respectively. There are occasional gaps in temporal coverage for the less accurate 'Original' and 'MAXBC' triggers because

we hedged our bets and scheduled tiling sequences during the burst response.

GRB 980527 was one of the first well-localized bursts observed by ROTSE-I. This is a very intense, spectrally hard burst lasting approximately 0.1 s. The first images were taken within 12 s of the burst start and consist of two groups of five exposures of 5 s and 25 s length with a tiling gap in between. After this, five 25 s exposures were taken centered on the subsequent MAXBC localization. Unfortunately, the MAXBC localization is more distant from the most likely position for this burst, reducing our coverage at later times. In addition, camera 'a' was not functioning which reduces our coverage to 86% (stat.+sys.). The only trigger localizations provided for both GRB 990323 and GRB 990808 were of the 'MAXBC' variety, and so our imaging begins more than 10 minutes after these bursts. Both GRB 991028 and GRB 991228 possess 'Original' and 'Final' localizations. GRB 991028 is a spectrally hard short burst and these on-line positions are a good match to that determined off-line by the BATSE team. Hardware behavior suffered in two ways for the GRB 991228 trigger response: camera 'c' did not take useable data, and camera 'd' exhibited a mild charge-transfer problem. For GRB 000201, we only triggered on the 'Final' localization since the 'Original' position was deemed unobservable by the automated scheduler. The best localization for this burst consists of an IPN diamond derived from BATSE, ULYSSES and NEAR data, and is well-covered by the ROTSE-I images. Observing conditions for all of these bursts were good.

The reduction of the data proceeds as in (Kehoe et al. 2000a). Raw images are dark subtracted and flat-fielded by using darks and sky-flats generated on the night of the trigger. Clustering of the corrected image is performed with SExtractor (Bertin and Arnouts 1996) utilizing a background mesh segmented by 32 pixel increments. Raw magnitudes are based on 5×5 pixel apertures. Astrometric calibration and determination of the overall zero-point for the image are performed by comparison to the Hipparchos catalog (Hog et al. 1998). During this step, a bad pixel template, derived from the raw darks for each camera, is used to flag objects containing such pixels within their apertures. A systematic error is assigned to the source based on the observed fluctuations of the constituent bad pixels.

Individual calibrated source lists are matched up to one another to form preliminary lightcurves. Any observation of an object is tagged as bad in which the position lies over one half pixel from the source's mean location. Final photometric calibration across the image is then performed by determining the median magnitude for a set of template sources for each 100 pixel $\times$ 100 pixel image subregion, and using these to derive a map of offsets and offset variances in each subregion. All objects are then corrected by a bilinear interpolation of this relative photometry map, and a systematic error is assigned based on the offset variance.

3. Analysis and Discussion

The analysis of the burst fields proceeded on two paths: a small field search applied to GRB 000201, and a wide field search applied to the other five. In both, candidate objects are rejected if they do not occur in at least one consecutive pair of observations. In addition, an object's individual observations are ignored if they are saturated or at an image edge. From here, the two analyses differ.

Because the IPN localization for GRB 000201 dramatically reduced the background for a counterpart search, we employed a loose lightcurve selection. During the observations in which a candidate is detected, there must be at least one pair of good measurements which exhibits a variation in excess of $0.5 + 5\sigma$, where σ is the sum in quadrature of the statistical and systematic errors of the two observations involved. Because it was the best localization early, we searched within the 1 σ (stat.) limits of the later BATSE LocBurst position. We have also checked the location of a purported optical counterpart detection (Boer et al. 2000). No counterparts were identified. An initial IPN localization became available on Feb. 9, and we searched within a surrounding box having sides with $\alpha = 138.75^o - 139.25^o$ and $\delta = 17.95^o - 18.45^o$. The final IPN diamond which was obtained later comprises the inner 20% of this region. We found no counterparts in this region.

This IPN-based analysis gives insufficient control of backgrounds in wide-field searches. To address this, we first attempted an image differencing approach on GRB 980527 (Kehoe et al. 2000a).

This method's effectiveness was reduced, however, because blending is not a critical problem in ROTSE images away from the galactic plane, and the typical PSF is very undersampled. In addition, it removes the diagnostic information present in the original image with which we can either correct occasional mild photometric variations, or flag problem observations. As a result, we perform our wide-field search by extending our IPN-based analysis with a more restrictive lightcurve variation selection, as well as a more stringent requirement on local observation quality. Individual observations are rejected if: a bad pixel lies within the aperture, there is a large offset from the mean position (ie.$>$ 0.5 pixel), photometry in the local image subregion has a large ($>$ 0.1 mag) standard deviation, or there are $<$ 5 template stars per local subregion. Lightcurve cuts were chosen based on a comparison of simulated bursts with power-law lightcurves vs. typical backgrounds observed in ROTSE trigger data. We require at least one variation passing a logical AND of $>$ 0.5 mag. and $> 5\sigma$ (stat.+sys.). In addition, we require that the overall lightcurve (using good observations only) differs from constant by a $\chi^2_{cl} > 3.0$ per degree-of-freedom, where the largest variation is excluded from the calculation. This last criterion also implies that the source is detected in 3 good, not necessarily consecutive, observations.

No candidates were observed for GRB 990323, GRB 990808 or GRB 991028 after these selections. A few objects passed the selection for GRB 980527, but most of these correspond to known sources in the USNO A-2.0 catalog (USNO 1998). Examination of the images for the remaining candidates revealed them to be incompletely removed bad pixels. For GRB 991228, the source of the candidates was solely due to a charge-transfer problem giving rise to spurious transients in the trailing charge. The limits for these bursts are shown in Figure 1, and are itemized in Table 2 for up to three discrete epochs.

All three short bursts have very prompt trigger responses, and two, GRB 980527 and GRB 991028, provide a probable coverage of the allowed error region. The earliest limits from these two bursts are 13.1 and 13.8 mag at 9.9 s and 12.2 s, respectively. Later limits range from magnitude 14 to 15. Our non-detections for these bursts, which have very different durations, suggest that short bursts do not usually give rise to optical emission brighter than 13th or 14th magnitude in the first few minutes after the burst. Unfortunately, we do not have data for the first 10 seconds of the burst which may be a critical phase for short duration events.

Among the three long duration bursts analyzed, two have a high coverage probability, and one (GRB 000201) has images starting soon after the burst. The best limits for this sample are 14.0 mag at 95.9 s and 15.8 mag late. The non-detection of a counterpart in these cases reinforces our previous conclusion that early optical emission from GRBs is not typically brighter than 14th magnitude, and it is fainter than 16th magnitude around 1 hour after the burst.

In an effort to compare this data to the only burst in which prompt optical emission has been observed, we have replotted the limits in Figure 2 after adjusting for their peak flux in 64 ms binning of the 50-300 keV BATSE data, as compared to GRB 990123. An optical burst from GRB 980527, GRB 981028 and GRB 000201 would have been observable if optical flux and gamma-ray flux were highly correlated.

More prompt optical data are clearly needed. This analysis, which is the first attempt in this direction, signals a hopeful future for more sensitive work. The methods described here are directly applicable to the ROTSE-III imaging which will be the mainstay of this effort in the future. It should now be possible to perform IPN-based searches to much deeper magnitudes than with ROTSE-I. More importantly for early optical study, we are now implementing an improved pipeline to find an optical transient in a fully automated and rapid way based on HETE-2 triggers.

We thank the BATSE team for their GRB data. We also thank the NEAR and ULYSSES teams for their GRB 000201 data. ROTSE is supported by NASA under *SR&T* grant NAG5-5101, the NSF under grants AST-9703282 and AST-9970818, the Research Corporation, the University of Michigan, and the Planetary Society. Work performed at LANL is supported by the DOE under contract W-7405-ENG-36. Work performed at LLNL is supported by the DOE under contract W-7405-ENG-48. Kevin Hurley is grateful for Ulysses support under JPL Contract 958056,

and for NEAR support under NASA grant NAG5-3500 and NAG5-9503.

REFERENCES

Hurley, K. 1992. in AIP Conf. Proc. 265, Gamma-Ray Bursts, ed. W. Paciesas and G. Fishman.

Kouvelioutou, C., et al. 1993, ApJ, 413, L101.

Dezalay, J., et al. 1992, in "Gamma-Ray Bursts", p304-309.

Nakar, E. and Piran, T. 2001. subm. to Mon. Not. R. Astron. Soc., astro-ph/0103192.

Kobayashi, S. 2000, ApJ, 545, 807.

van Putten, M., and Ostriker, E. 2001, acc. by ApJL, astro-ph/0010440

Cline, D., Matthey, C., and Otwinowski, S. 1999. ApJ, 527, 827.

Metzger et al. 1997. IAU Circ. 6676.

Kulkarni et al. 1998. Nature, 393:35-39.

Akerlof, C., et al. 1999, Nature, 398, 400

Feroci, M. et al. 1997. In Proc. SPIE Vol. 3114, *EUV, X-ray, and Gamma-Ray Instrumentation for Astronomy VIII*, 186+.

Park, H., et al. 1999, AApS, 138, 577.

Hurley, K., et al. 1999, ApJS, 122, 497.

Akerlof, C., et al. 2000, ApJ, 532, L25.

Barthelmy, S. et al. 1995. *Astrophysics and Space Science,* **231**:235–238.

Barthelmy, S. et al. 1998. http://gcn.gsfc.nasa.gov/gcn/.

Kehoe, R. et al. 2000, in the STScI May Symp., The Largest Explosions Since the Big Bang: Supernovae and Gamma Ray Bursts, ed. M. Livio, N. Panagia, & K. Sahu (Baltimore:STScI)

Paciesas, W., et al. 1999, ApJS, 122, 465.

Boer, M., Atteia, J., and Klotz, A., 2000, GCN Circ. 535

Kehoe, R. Wren, J., and Lee, B., 2000, GCN Circ. 536

Bertin, E., & Arnouts, S. 1996, A&AS, 117, 393

Hog, E., et al, 1998, A&A, 335, L65.

USNO catalog, http://www.nofs.navy.mil/.

This 2-column preprint was prepared with the AAS LaTeX macros v5.0.

Fig. 1.— m_{ROTSE} limiting magnitudes vs. time after gamma-ray onset. GRB 990123 optical burst detections are shown for comparison.

Fig. 2.— Flux rescaled limits for six GRBs vs. time after gamma-ray onset. If optical emission were positively correlated with peak gamma-ray flux, ROTSE-I would have detected optical bursts for GRB 980527, GRB 991028, GRB 991228, and GRB 000201.

GRB	trigger	T_{50}	T_{90}	ϕ_{peak}	fluence	coverage	t_+
980527	6788	0.049	0.092	21.1	6.5	86(70)	12.19
990323	7489	85.0	118.8	0.51	28.2	20	640.62
990808	7704	42.0	75.8	0.81	8.9	75	716.38
991028	7827	0.5	2.3	1.2	0.6	70	9.90
991228	7922	0.27	0.42	2.8	1.0	5	17.65
000201	7976	48.3	95	3.3	145	100	85.89

Table 1: Characteristics of six bursts responded to by ROTSE-I. Corresponding information for GRB990123 is given in (**?**)). The columns specify: GRB date, BATSE trigger number, duration in seconds where endpoint fluxes are 50% of peak, duration where endpoint fluxes are 10% of peak, peak flux (ϕ_{peak}, in $photons/cm^2/s$), fluence ($\times 10^{-7} erg/cm^2$), coverage of the GRB probability (%), and start time (t_+, in sec.) for first image recorded. The peak flux is taken using 64 ms binning, except for GRB 990323 and GRB 990808 for which only 1024 ms binning was available. Coverages for epochs with pointings different than the first epoch are indicated in parentheses.

date	t_1	Δt_1	$m_{ROTSE}(t_1)$	t_2	Δt_2	$m_{ROTSE}(t_2)$	t_3	Δt_3	$m_{ROTSE}(t_3)$
980527	14.69	5	13.76	208.35	25	14.84	617.64	25	14.98
990323	-	-	-	650.62	20	14.80	1048.06	80	15.59
990808	-	-	-	726.38	20	14.48	1122.25	80	15.10
991028	12.40	5	13.06	200.02	20	13.65	397.85	80	13.85
991228	20.15	5	13.71	81.49	20	14.78	666.16	80	15.33
000201	95.89	20	14.03	680.00	20	15.14	2871.64	365.6	15.76

Table 2: Summary of limits for six bursts responded to by ROTSE-I. Columns list up to three epochs (middle of exposure, in sec.), and their exposure length (sec.) and sensitivity.

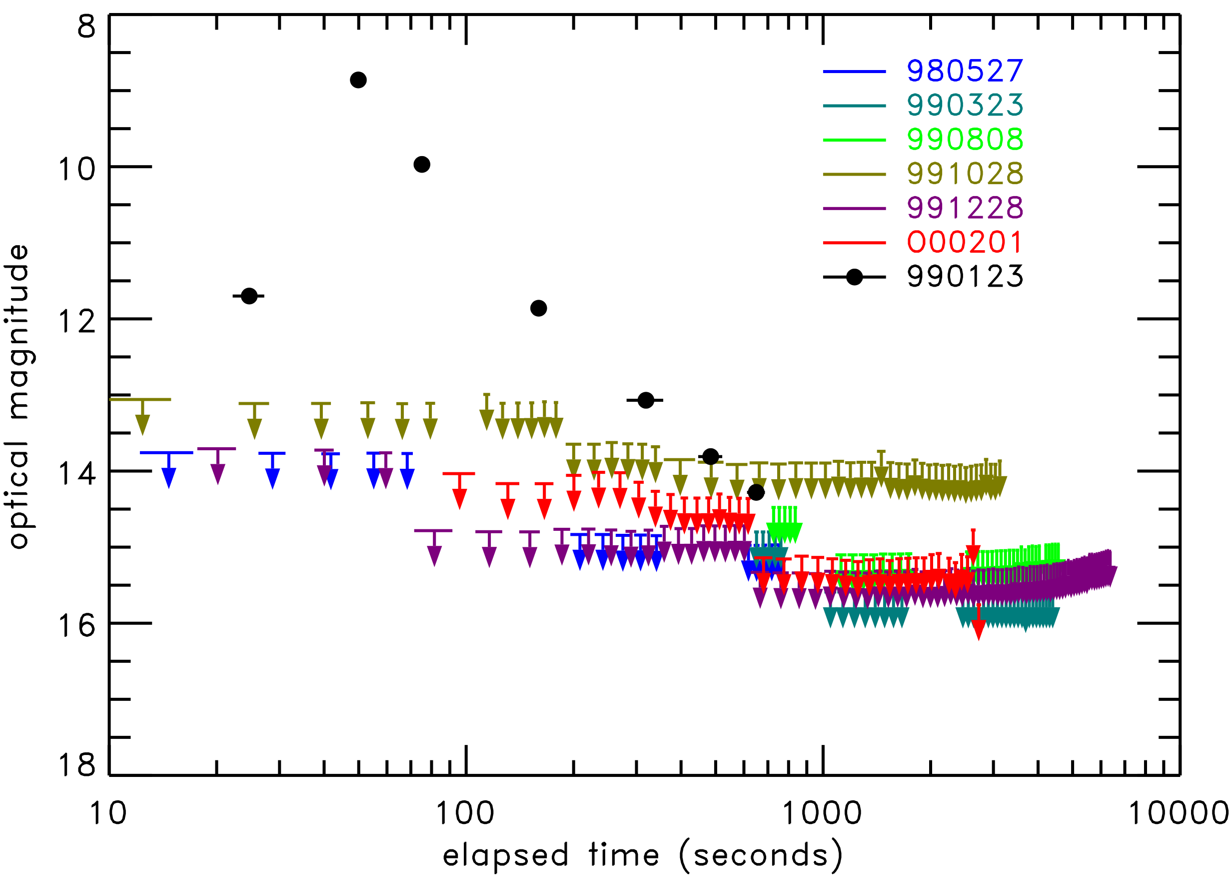

980527
990323
990808
991028
991228
000201
990123
optical magnitude
elapsed time (seconds)
8
10
12
14
16
18
10
100
1000
10000

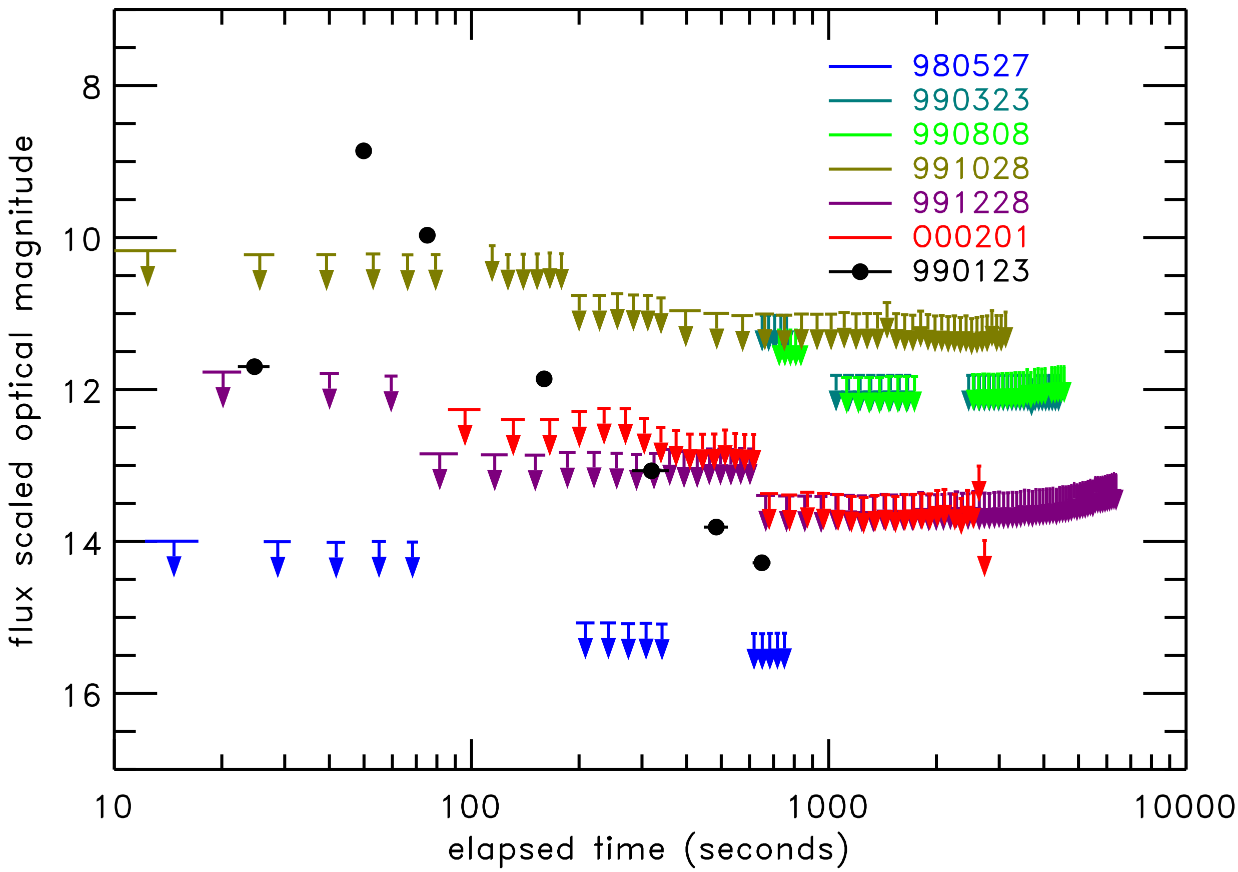

980527
990323
990808
991028
991228
000201
990123
8
10
12
14
16
flux scaled optical magnitude
10
100
1000
10000
elapsed time (seconds)